A role for keratins in supporting mitochondrial organization and function in skin keratinocytes

Kaylee Steen[1], Desu Chen[2], Fengrong Wang[1], Ritankar Majumdar[3], Song Chen[3], Surinder Kumar[4], David B. Lombard[4,5], Roberto Weigert[2], Carole A. Parent[1,3,5], and Pierre A. Coulombe[1,5,6,*]

[1] Department of Cell and Developmental Biology, University of Michigan Medical School, Ann Arbor, MI 48109, USA.

[2] Laboratory for Cellular and Molecular Biology, Center for Cancer Research, National Cancer Institute, National Institutes of Health, Bethesda, Maryland.

[3] Department of Pharmacology, University of Michigan Medical School, Ann Arbor, MI 48109, USA.

[4] Department of Pathology, University of Michigan, Ann Arbor, MI 48109, USA.

[5] Rogel Cancer Center, University of Michigan, Ann Arbor, MI 48109, USA.

[6] Department of Dermatology, University of Michigan Medical School, Ann Arbor, MI 48109, USA.

*To whom correspondence should be addressed: Pierre A. Coulombe, Ph.D., Dept. of Cell and Developmental Biology, University of Michigan Medical School, 109 Zina Pitcher Place, Ann Arbor, MI 48109, USA. ; E-mail: coulombe@umich.edu ; Tel: 734-615-7509.

Present addresses:

Fengrong Wang: Department of Microbiology and Immunology, University of Michigan Medical School, Ann Arbor, MI 48109, USA

Kaylee Steen: Office of Research, University of Michigan Medical School, Ann Arbor, MI 48109, USA

Running title: **Keratins regulate mitochondrial dynamics and function**

Keywords: Skin, keratinocytes, keratin, mitochondria, mitochondrial dynamics, oxidative stress, wound repair, pachyonychia congenita, genodermatoses, live cell imaging.

Abstract

Mitochondria fulfill essential roles in ATP production, metabolic regulation, calcium signaling, generation of reactive oxygen species (ROS) and additional determinants of cellular health. Recent studies have highlighted a role for mitochondria during cell differentiation, including in skin epidermis. Furthermore, the observation of oxidative stress in keratinocytes from *Krt16* null mouse skin, a model for pachyonychia congenita (PC) -associated palmoplantar keratoderma, prompted us to examine the role of K16 protein and its partner K6 in regulating the structure and function of mitochondria. Electron microscopy revealed major anomalies in mitochondrial ultrastructure in late stage, E18.5, K*rt6* null embryonic mouse skin. Follow-up studies utilizing biochemical, metabolic, and live imaging readouts showed that, relative to controls, skin keratinocytes null for *Krt6* or *Krt16* exhibit elevated ROS, reduced mitochondrial respiration along with significant alterations in the length, intracellular distribution and movement of mitochondria within the cell. These findings highlight a novel role for K6 and K16 in regulating mitochondrial morphology, dynamics and function and shed new light on the causes of oxidative stress observed in PC and related keratin-based skin disorders.

Introduction

Keratinocytes, the primary cell type that constitutes the skin epidermis, must be able to proliferate, move unidirectionally, assemble and remodel strong adhesive sites as they differentiate, and resist mechanical stress. A major family of proteins that impacts all of these functions are the keratin (K) intermediate filaments (IFs), which are regulated in a tissue type-, differentiation- dependent and context- specific manner [1,2]. The human genome features 54 distinct and conserved keratin genes that are partitioned into type I and type II subtypes based on IF sequences [3]. Type I and II keratin genes are expressed in a pairwise fashion and their protein products interact obligatorily to form heteropolymeric 10-nm wide IFs [2]. Mutations in keratin genes have been linked to a variety of chronic skin disorders with an even wider range of pervasive phenotypes [4]. One such keratin pair, the type II K6 and type I K16, is primarily expressed in ectoderm-derived epithelial appendages in adult skin under normal conditions [2,5,6]. The interfollicular epidermis, interestingly, does not express either K6 or K16 unless it experiences injury, UV exposure, or other stresses [4,7,8]. Mutations in either *KRT6A*, *KRT6B*, *KRT6C* or *KRT16* (usually, dominantly-acting missense alleles) can cause PC [9-11]. The most clinically significant aspect of PC is palmoplantar keratoderma (PPK), which are acutely painful and featured with thick calluses developing in the palms and especially soles as a result of oxidative stress and misregulated innate immunity and epidermal homeostasis [7,12].

In addition to forming filamentous networks, keratins are known to regulate signaling pathways through protein-protein interactions and to modulate organelle processes [13]. For instance, there is an emerging connection between mitochondrial biology and IFs that has the potential to alter the cellular levels of ROS and metabolic flux [13-15]. As mentioned above, our laboratory has previously reported that normal redox balance requires functional K16 via Nrf2 activation and glutathione synthesis. In the case of PC-related PPK, an imbalance in redox homeostasis precedes the appearance of lesions and can be rescued using a Nrf2 activator [12]. These observations prompted us to investigate mitochondria as a source of dysfunction since this organelle is a major hub of ROS production, is critical for cell energetics and redox homeostasis, and we previously reported on ulrtrastructural anomalies in late embryonic skin of *Krt5* null mice [16]. Besides, K8, a type II keratin expressed in simple epithelia, has recently been shown to modulate mitochondrial network formation [14,15]. We found that lack of K16 and, to a greater extent, lack of K6 impair mitochondrial cristae formation, respiration, and dynamics in skin keratinocytes. These observations suggest that disruption of mitochondrial-keratin interactions, which in turn leads to impaired cellular and redox homeostasis, is related to oxidative stress that precede PPK lesions.

Results

As previously reported, mice homozygous for a *Krt6a/Krt6b* double-null allele are born with the expected frequency but rapidly develop oral lesions that hampers their postnatal growth and results in their untimely death within a week post-birth [17]. We first used transmission electron microscopy (TEM) to compare the ultrastructural features of epidermis and, in particular, mitochondria in late stage (E18.5) embryonic *Krt6a/Krt6b* null and WT back skin. Low magnification surveys of epoxy-embedded tissue sections show that the epidermis of *Krt6a/Krt6b* homozygous null mice is intact and shows a normal morphology (Supplemental Fig. 1). In contrast, examination at higher magnifications reveals that, relative to control, mitochondria in epidermal keratinocytes lacking both keratins 6a and 6b proteins (K6a/K6b) exhibit several anomalies with respect to shape and cristae organization (Figures 1A-B). First, most mitochondria from the skin of mutant animals exhibit a swollen appearance and a circular shape rather than the elongated and electron-dense morphology seen in normal control tissue (Figure 1A), along with cristae that are highly disorganized and partitioned to the edges of the organelle (Figure 1B, left panel). These findings suggest that mitochondria are in a compromised state in the absence of K6a/K6b proteins. A second characteristic observed in *Krt6a/Krt6b* null embryonic skin is that those mitochondria showing a typical elongated shape frequently appear to have a polarized ultrastructure, with one region exhibiting normal cristae and the opposite end contained highly disorganized cristae (Figure 1B, right panel). While this could be a result of inefficient fission and fusion disorganized cristae (Fig 1B, right panel [18-20], we did not observe any major expression differences in relevant biomarkers (*Mfn1*, *Mfn2*, *Opa1* and *Drp1*) with the exception of a small increase in *Mfn2* in *Krt6a/Krt6b null* keratinocytes compared to *WT* cells (Figure 1D). We did observed, there also was a modest trend towards lower mRNA levels for the mitochondrial markers cytochrome c oxidase subunit 4 (COX4), succinate dehydrogenase (SDH), translocase of the inner membrane (Tim23), complex III subunit 2 (COR2), and pyruvate dehydrogenase (PDH), in *Krt6a/Krt6b null* keratinocytes relative to *WT*, with Tim23 and PDH reaching statistical significance (Figure 1C). Finally, we did not observe any change in mitophagy markers responsible for mitochondrial turnover (data not shown), which is consistent with data gathered from keratinocytes of PC patients with K6a mutations ([11]; see Discussion). Of note, we previously reported on the occurrence of similar ultrastructural defects in mitochondria from *Krt5 null* E18.5 mouse epidermis [16]. Furthermore, the loss of another IF protein, desmin, was found to induce mitochondrial swelling and matrix disruption in cardiac muscle. Importantly, the mitochondria in desmin-null cardiac muscle displayed a very similar phenotype to the *Krt6a/Krt6b* null mitochondria as shown Figure 1C [21]. This suggests that as is the case for other intermediate filaments, the K6/K16 filament network likely plays a direct role in mitochondrial architecture.

Keratin proteins physically interact with several cellular organelles [14,15,22,23], including mitochondria. We next compared the subcellular distribution of K16, for which we have a high titer (monospecific) antibody [5,24], to that of PDH using high resolution confocal microscopy (Airyscan technology) in *WT* newborn mouse skin keratinocytes in primary culture. The signal for K16 closely aligns with that of PDH, which otherwise is polarized towards the perinuclear space (Figures 2A-2B). In follow-up studies using conventional confocal microscopy, we found

that the absolute spatial distribution of the mitochondria (as measured by PDH) is altered when the K6/K16 network is ablated. As seen in Figure 2B, the PDH signal is redistributed to the entire cytoplasm in mouse *Krt6a/Krt6b* null keratinocytes in primary culture, with a higher PDH signal at the cell periphery compared to the perinuclear localization in *WT* keratinocyte controls (Figure 2B). This effect was also observed in spontaneously immortalized keratinocytes (SIMEKs) lacking *Krt16* (data not shown). These findings suggest that keratin IFs containing K6 may directly or indirectly impact the organization of mitochondria in epidermal keratinocytes. Loss of the K6/K16 network leads to a differential dispersion of mitochondria throughout the cell, which has the potential to disrupt the physiological signaling capacity of this organelle (see Discussion).

Cells rely on the electron transport chain (ETC) of the mitochondria to produce ATP through the reduction and oxidation of ETC protein complexes from electrons donated from the TCA cycle [18]. Efficient operation of this complex process requires that cristae be densely packed inside mitochondria to keep the ETC complexes close together for electron transport [25,26]. If such a continuity is not maintained, electrons can move back into the mitochondrial matrix, react with molecular oxygen and produce excess ROS [18,27,28]. The observation of significantly abnormal mitochondrial ultrastructure led us to hypothesize that the absence of either K6a/K6b or K16 protein leads to the occurrence of imbalances in ROS levels. To test this, we measured total ROS in *WT* and *Krt6a/Krt6b* null keratinocytes cultured under normal and stressed conditions through the exposure to tert-butyl hydrogen peroxide. Cells lacking K6a/K6b consistently produced more ROS relative to *WT* under both baseline and stressed conditions (Supplemental Figure 2A), supporting the TEM data from back skin showing disorganized cristae. A similar trend was observed in *Krt16* null keratinocytes in primary culture, though it did not reach statistical significance (Supplemental Figure 2B). We repeated this assay in spontaneously immortalized cells isolated from *WT* and *Krt16 null* mice and found that, similar to what is seen in *Krt6a/Krt6b null* keratinocytes, immortalized cells lacking *Krt16* displayed higher levels of ROS compared to *WT* (Supplemental Figure 2C).

ROS have been implicated in many forms of cellular dysfunction and can directly damage mitochondria [29-31]. To explore how increased ROS affects mitochondrial function in cells lacking either K6a/K6b or K16, we measured mitochondrial respiration using the Seahorse Mito Stress Test Kit. Keratinocytes isolated from both *Krt6a/Krt6b null* and *Krt16 null* mice (P1) showed a significant reduction in basal and maximal respiration compared to *WT* cells. Null keratinocytes also displayed a reduced proton leak (Figure 3A), suggesting that there may be an overall reduction in uncoupling protein activity or increased permeability of the inner mitochondrial, reducing over electron movement across the ETC [26,32].. This finding was further supported by reduced membrane potential as measured by TMRE fluorescence in both *Krt6a/Krt6b null* and *Krt16 null* keratinocytes (Figure 3B). Interestingly, other intermediate filaments, namely vimentin, have also been shown to maintain membrane potential and loss of this interaction alters mitochondrial positioning and physiological activity [33].

Mitochondria are highly dynamic organelles that constantly undergo fission and fusion to create complex networks that help regulate several cellular functions in response to exogenous

signals [19,34]. Moreover, respiration and ROS production are regulated by and can impact mitochondrial dynamics [18,29,35-37]. To assess whether and how K6/K16 alter mitochondria dynamics, we labeled skin keratinocytes in culture with MitoTracker Red and performed live cell imaging in real time to monitor mitochondrial movement under normal cellular conditions. In keratinocytes null for either keratin, mitochondrial shapes showed no alteration in size or circularity but exhibited an increased speed of movement [38] (data not shown and Figure 4. Representative movies and average mitochondrial speed as a function of mitochondrial size are shown in Supplemental videos 1-4 and Supplemental Figure 3, respectively). The increased speed was unrelated to the size of mitochondrial profiles (represented by the x-axis), although smaller mitochondrial shapes showed a greater rate of movement in the two knockout genotypes compared to the normal keratinocytes (Supplemental Videos 1-4). Furthermore, our data also show the large heterogeneity of mitochondrial populations even within the same cell type and individual cell (Supplemental Videos 1-4). Besides, mitochondria in *Krt6a/Krt6b*-null and Krt16-null keratinocytes also appeared to move in a disorganized or random fashion, but we were unable to quantify this behavior. Overall, these data demonstrate a clear difference in the motility of the mitochondrial shapes in keratinocytes lacking K6 or K16. While the live imaging performed does not directly measure mitochondrial fission and fusion rates, it extends the findings of disrupted mitochondrial ultrastructure (Figure 1) and reduced respiration (Figure 3), pointing to a state of mitochondrial instability.

Collectively these findings indicate that K6/K16-containing IFs provide a type of scaffold that maintains the integrity of mitochondrial structure, function, and organization within skin keratinocytes. Whether this action is direct or indirect is unclear. A yeast-two hybrid screen showed that the protein trichoplein (TCHP) selectively binds type I and type II intermediate filaments, with the greatest binding strength shown for K16 and K18 [13,14]. TCHP has been proposed to mediate keratin binding to mitochrondria. We could not produce reliable evidence for a physical interaction between TCHP and K16 in skin keratinocytes, unfortunately, owing in part to the unavailabitlity of of good antibody to TCHP (data not shown) – addressing this issue awaits the availability of suitable reagents.

Discussion

Keratin proteins play a multifaceted role in keratinocyte homeostasis, and mutations in keratin genes lead to a diverse range of phenotypic outcomes. The K6/K16 keratin pairing, which is robustly wound-inducible, supports and promotes a number of cellular functions including structural integrity [17,24,39], cell migration [8,40], keratinocyte differentiation [41], regulation of innate immunity [7] and redox homeostasis [12,42]. Disruption of many of these cellular functions is poised to play a role in the pathophysiology of PC, in particular, in oral and palmoplantar keratoderma lesions [43]. Mitochondria represent the main cellular protagonist for regulation of ROS, which it achieves mainly via preserving the integrity and promoting the efficiency of the electron transport chain. Silvander *et al*. [14] recently reported that loss of keratin 8 reduce mitochondrial membrane potential and ATP production in pancreatic β-cells, a novel role that involves an interaction with TCHP. Furthermore, Nishizawa *et al*. [13] provided evidence that K6 and especially K16 physically interact with TCHP. Here show that K6 and K16

regulate the organization and function of mitochondria in skin keratinocytes, a novel finding that has potential significance not only for the keratinocyte differentiation [36] and epithelial homeostasis [11,44,45], but also for the pathophysiology of keratin mutation-based skin epithelial disorders [4,10-12,39].

ROS levels are significantly higher in keratinocytes null for *Krt6a/Krt6b* or *Krt16* relative to wildtype controls. These findings correlate with the reduced mitochondrial basal and maximal respiration in both the *Krt6a/Krt6b* and *Krt16* ablated states as measured by Seahorse analysis. The latter also indicated that there is reduced proton leak in the two keratin null settings, which is further supported by the reduced membrane potential prevailing in mitochondria. These findings are also consistent with the highly damaged and disorganized cristae observed in mitochondria of *Krt6a/Krt6b null* keratinocytes. Mitochondria tend to be localized to the perinuclear cytoplasm in wildtype keratinocytes but show a broader dispersion in keratinocytes lacking K6a/K6b or K16. Of note, keratin filaments themselves readily concentrate to the perinuclear region, particularly in suprabasal keratinocytes of surface epithelia [22,23]. Accordingly, alterations in keratin filament properties resulting from the loss of either K6a/K6b or K16 may prevent the mitochondria from concentrating near the nucleus. Importantly, the subcellular localization of mitochondria is known to have a major impact on cell signaling and function, including migration, calcium signaling, and gene expression [46-50]. The alteration of this steady state is an exciting area for future studies to determine the associated effects on keratinocyte function. ROS production and mitochondrial function are also closely linked to the latter's dynamics and network formation, and indeed differences were measured in the motility of mitochondria in *Krt6a/Krt6b*-null and *Krt16*-null keratinocytes relative to *WT*. Through the use of MitoTracker for live cell imaging, we determined that mitochondria exhibit enhanced movement speed in skin keratinocytes lacking K6a/K6b or K16. These data suggest that keratins help stabilize mitochondria spatially and structurally within keratinocytes, and that disrupting these processes has significant consequences for cell signaling, bioenergetics, and redox homeostasis [18-20,51].

Our findings significantly extend a recent study showing that mitophagy turnover is impaired in cultures of immortalized keratinocytes derived from individuals with PC [11], thus adding to the evidence that anomalies in mitochondria and in redox balance may play a significant role in the pathophysiology of PC-associated PPK. They also add to a growing body of evidence linking keratin [14] and other types of IFs, notably vimentin and desmin, to mitochondrial regulation and function [21,33,52,53]. Like microtubules and actin filaments, intermediate filaments are also required in controlling mitochondrial motility, likely through stabilization, which in turn regulates the site of ATP production, calcium signaling and metabolic alteration [53-56]. Our data demonstrating increased mitochondrial speed as a result of K6 and K16 ablation strongly supports those findings. However, there are many unresolved issues that remain. First, while others provided evidence that K16 and K6 can bind to trichoplein, a candidate mitochondrial linker protein [13,14], there is still a need to definitively identify the mechanism in which keratin filaments interact with the mitochondria. Secondly, we do not know whether the mitochondrial dysfunction is leading to increased ROS production or if the damage is a result of an already established oxidative stress. This is significant because activation of oxidative stress

pathways precedes PPK lesions in mice and reducing oxidative stress in PC patients ameliorates symptoms [12,42]. These finding reported herein provide a platform to answer these questions and provide a truer picture of keratins active role in regulating mitochondrial function, structure and dynamics.

Materials and Methods

Mouse handling

All experiments involving mice were reviewed and approved by the Unit for Laboratory Animal Medicine (ULAM) at the University of Michigan. The *Krt6a/Krt6b* null [17] and *Krt16* null [24] mouse strains (C57BL/6 background) were maintained under specific pathogen–free conditions, fed chow and water ad libitum, and bred and genotyped as described. All studies with E18.5 back skin tissue and newborn skin (P1-P2 pups) keratinocytes in primary culture were performed using littermates with a *WT* or homozygous *null* genotype.

Reagents

Primary antibodies used includes anti-PDH (Abcam), Anti-FLAG® M2 Magnetic Beads (Sigma-Aldrich), -TCHP (abcam), -β-actin, -K16 [5] and -K6 [6], MitoTracker CMXRos (ThermoFisher) was used for live cell imaging of the mitochondria. Secondary antibodies used included HRP-conjugated secondary antibodies (Sigma-Aldrich) and Alexa Fluor 488, Alexa Fluor 594 and Alexa Fluor 647 (ThermoFisher).

Tissue preparation

Krt6a/Krt6b heterozygous mating pairs were set up and E18.5 pups were harvested for genotyping. [57]. Tissue sectioning for immunostaining was performed by submerging back skin into OCT (Sakura Finetek), freezing at -20°C, and preparing 5uM sections using the CryoStar NX50 (Thermo Scientific) and stained as described below. TEM tissue preparation is described below.

Keratinocyte culture

WT and *Krt6a/Krt6b null* and *WT* and *Krt16 null* littermates were taken at P1. The skin was removed and left in 0.25% Trypsin overnight at 4°C, and following day the keratinocyte isolation was performed as described by Rotty and Coulombe, 2012 [8]. The cells were counted and seeded on collagen I coated plates based on each experimental need in differentiation promoting mKER media for two days unless specified otherwise.

Mitochondrial respiration

The Seahorse XFe96 analyzer was used to measure mitochondrial respiration following the protocol from the Agilent Seahorse XF Cell Mito Stress Test kit. Cells were seeded at 4×10^4 and the mKER media was replaced with the Agilent Base Medium with 1mM sodium pyruvate and 2mM glutamine prior to the assay. The data was normalized to total cells using Hoechst dye in the final port injection and transferred to the Cytation 5 for analysis (BioTek).

Measurement of reactive oxygen species

Keratinocytes were cultured in primary conditions from *WT* and *Krt6a/Krt6b null* and *WT* and *Krt16 null* littermates. Cells seeded in the Corning™ 96-Well Clear Bottom Black Polystyrene Microplates at a cell density of 5×10^4. Due to the fast-growing nature of the immortalized cells, only 2.5×10^4 cells were seeded for the *WT* and *Krt16 null* SIMEKs and followed the same procedure. The protocol from the abcam DCFDA cell ROS detection assay kit was used to measure total cellular ROS at baseline and with increasing concentrations of Tert-Butyl Hydrogen Peroxide.

Measurement of mitochondrial membrane potential

Keratinocytes were isolated from *WT* and *Krt6a/Krt6b null* and *WT* and *Krt16 null* littermates and seeded in the Corning™ 96-Well Clear Bottom Black Polystyrene Microplates at a cell density of 7×10^4. Following 48 hours of culturing, cells were incubated with 500nM of TMRE dye for 30 minutes followed by two washes with PBS containing 0.2% BSA. Fluorescence was measured at Ex/Em = 549/575 nm and normalized to cell number using the CyQUANT kit (ThermoFisher). Normalization was done by aspirating the media and freezing the cells at -80°C overnight. The cells were then labeled with CyQuant dye to measure total DNA.

Analysis of mitochondrial dynamics

Live cell imaging was performed to track the mitochondrial dynamics in *WT*, *Krt6a/Krt6b null* and *Krt16 null* keratinocytes. Cells were seeded in Collagen I coated wells at a density of 50K cells to reach about 60-70% confluency in order to image individual cells (Nunc™ Lab-Tek™ II Chambered Coverglass with a No. 1.5 borosilicate glass bottom for 48hrs). Prior to imaging, cells were incubated in Phenol red-free DMEM 0.5% BSA media containing 50nM of MitoTracker red for 15 minutes at 37°C. Cells were then washed once with Phenol red-free DMEM 0.5% BSA media and imaged using the Zeiss Airyscan LSM 880. Videos were taken with a 0.11 laser power, 0.5ms intervals, and 500 cycles with Airyscan processing. Due to the limitation of imaging, we were not able to resolve individual mitochondria. The objects segmented and measured most likely represent clusters of mitochondria (mitochondrial shapes). For each time frame mitochondrial shapes were segmented using the snake algorithm, an active contour model implemented with custom MATLAB scripts. In brief, this algorithm defined the outlines of mitochondrial shapes by a set of representative points along the boundary, i.e., “snakes” [ref: C. Xu, J.L. Prince, Snakes, shapes, and gradient vector flow, Image Processing, IEEE Transactions on 7(3) (1998) 359-369]. Snake contours were initiated with the convex hulls of the objects and converged to fit the boundary in the energy minimization iterations defined by force fields determined by brightness gradient of the fluorescence. Parameters used to identify outlines of mitochondrial shapes were: 1) the snake elasticity parameter α (0.01), 2) the viscosity parameter γ (0.05), and 3) the external force weight κ (0.5). Two mitochondrial shapes were considered the same object if they overlapped for more than 60% in two successive frames. Mitochondrial shapes that appear to fragment or fuse in successive frames were excluded from the quantification. Speed of the center of mass and the area of the tracked objects were determined.

Transmission electron microscopy

E18.5 back skin from *WT* and *Krt6a/Krt6b null* littermates were placed flat at the bottom of a 24-well plate and treated with 1mL of fixative (2.5% glutaraldehyde, 3% paraformaldehyde in Sorenson's buffer). The samples were then given to the University of Michigan's Microscopy and Image Analysis Laboratory (MIL) core for sample preparation. Mitochondrial topography was imaged using the JEOL 1400 Plus TEM at the MIL.

Indirect immunofluorescence

Immunostaining (indirect immunofluorescence) was performed on keratinocytes and epidermal back skin tissue sections. Samples were fixed in 4% paraformaldehyde for 10 minutes at room temperature, washed in PBS, blocked in 5% normal goat serum/0.1% Triton X-100/ PBS for 1 hour at room temperature, incubated in primary antibody solution overnight at 4°C, washed in PBS, incubated in secondary antibody solution for 1 hour, incubated with DAPI for 5 minutes, washed in PBS, and mounted in Fluor- Save Reagent Mounting Medium (EMD Millipore) before visualization using a Zeiss LSM 800 fluorescence confocal microscope. To quantify the mitochondrial PDH distribution throughout the cell, the nucleus and the cell boundaries were manually segmented with Fiji. Each boundary loop was then smoothed in MATLAB and 100 points on the boundary with even spacing were picked to partition the loop into 100 sections. The points on the cell boundary were linked to corresponding points on the cell nucleus boundary, keeping the circular order of the points and the total distance between paired points at the minimum. In this way, the area between the nucleus and the cell boundary was segmented into 100 regions. For each region (and the associated boundary points) the local distance between the nucleus and the cell boundary was defined as the distance between the middle points of the local nucleus and cell boundary sections. The distance of each pixel in the segmented regions to the nucleus was defined as the distance between the pixel to the middle point of the local nucleus boundary section. As some cells touched other cells, only the regions with cell boundary not touching other cells were manually selected for further analysis. To quantify the average PDH fluorescence intensity with respect to the distance to the nucleus, the distance was binned every 10 pixels (1.6 μm). The average PDH fluorescence intensity of pixels in each distance bin was then calculated.

Biochemical analyses

RNA was isolated from primary keratinocytes cells using the NucleoSpin RNA kit (Macherey-Nagel) followed by cDNA preparation (iScript cDNA synthesis kit; Bio- Rad). Primer information can be found in Supplemental Table 1 (all primers are designed against the *mus musculus* RefSeq through the NCBI database). K16-flag protein (C-terminally tagged) was made using the pcDNA™3.1 Directional TOPO™ Expression Kit (ThermoFisher) using primers for the mouse *Krt16* gene with flag peptide sequence on the 3' end (Supplemental Table 1).

Statistical analyses.

All statistical analyses, unless indicated elsewhere, were performed using a two-tailed Student's *t* test.

Acknowledgements

We thank Samarth Setru for his work on keratin 16 and other members of the Coulombe laboratory for support. These studies were supported by R01 grants AR044232 and AR042047 (to P.A. Coulombe) and R01 grant GM101171 (to D.B. Lombard) by the National Institutes of Health.

References

1. Fuchs E, Green H: **Changes in keratin gene expression during terminal differentiation of the keratinocyte**. *Cell* 1980, **19**:1033-1042.
2. Fuchs E: **Keratins and the skin**. *Annu Rev Cell Dev Biol* 1995, **11**:123-153.
3. Schweizer J, Bowden PE, Coulombe PA, Langbein L, Lane EB, Magin TM, Maltais L, Omary MB, Parry DA, Rogers MA, et al.: **New consensus nomenclature for mammalian keratins**. *J Cell Biol* 2006, **174**:169-174.
4. McGowan KaC, P.: **The wound repair-associated keratins 6, 16, and 17. Insights into the role of intermediate filaments in specifying keratinocyte cytoarchitecture**. *Subcell Biochem* 1998, **31**:31.
5. Bernot KM, Coulombe PA, McGowan KM: **Keratin 16 expression defines a subset of epithelial cells during skin morphogenesis and the hair cycle**. *J Invest Dermatol* 2002, **119**:1137-1149.
6. McGowan K, Coulombe PA: **The wound repair-associated keratins 6, 16, and 17. Insights into the role of intermediate filaments in specifying keratinocyte cytoarchitecture**. *Subcell Biochem* 1998, **31**:173-204.
7. Lessard JC, Pina-Paz S, Rotty JD, Hickerson RP, Kaspar RL, Balmain A, Coulombe PA: **Keratin 16 regulates innate immunity in response to epidermal barrier breach**. *Proc Natl Acad Sci U S A* 2013, **110**:19537-19542.
8. Rotty JD, Coulombe PA: **A wound-induced keratin inhibits Src activity during keratinocyte migration and tissue repair**. *J Cell Biol* 2012, **197**:381-389.
9. Leachman SA, Kaspar RL, Fleckman P, Florell SR, Smith FJ, McLean WH, Lunny DP, Milstone LM, van Steensel MA, Munro CS, et al.: **Clinical and pathological features of pachyonychia congenita**. *J Investig Dermatol Symp Proc* 2005, **10**:3-17.
10. McLean WH, Rugg EL, Lunny DP, Morley SM, Lane EB, Swensson O, Dopping-Hepenstal PJ, Griffiths WA, Eady RA, Higgins C, et al.: **Keratin 16 and keratin 17 mutations cause pachyonychia congenita**. *Nat Genet* 1995, **9**:273-278.
11. Lehmann SM, Leube RE, Schwarz N: **Keratin 6a mutations lead to impaired mitochondrial quality control**. *Br J Dermatol* 2019.
12. Kerns ML, Hakim JM, Lu RG, Guo Y, Berroth A, Kaspar RL, Coulombe PA: **Oxidative stress and dysfunctional NRF2 underlie pachyonychia congenita phenotypes**. *J Clin Invest* 2016, **126**:2356-2366.
13. Nishizawa M, Izawa I, Inoko A, Hayashi Y, Nagata K, Yokoyama T, Usukura J, Inagaki M: **Identification of trichoplein, a novel keratin filament-binding protein**. *J Cell Sci* 2005, **118**:1081-1090.
14. Silvander JSG, Kvarnstrom SM, Kumari-Ilieva A, Shrestha A, Alam CM, Toivola DM: **Keratins regulate beta-cell mitochondrial morphology, motility, and homeostasis**. *FASEB J* 2017, **31**:4578-4587.
15. Tao GZ, Looi KS, Toivola DM, Strnad P, Zhou Q, Liao J, Wei YQ, Habtezion A, Omary MB: **Keratins modulate the shape and function of hepatocyte mitochondria: a mechanism for protection from apoptosis**. *Journal of Cell Science* 2009, **122**:3851-3855.
16. Alvarado DM, Coulombe PA: **Directed expression of a chimeric type II keratin partially rescues keratin 5-null mice**. *J Biol Chem* 2014, **289**:19435-19447.

17. Wong P, Colucci-Guyon E, Takahashi K, Gu C, Babinet C, Coulombe PA: **Introducing a null mutation in the mouse K6alpha and K6beta genes reveals their essential structural role in the oral mucosa**. *J Cell Biol* 2000, **150**:921-928.
18. Buck MD, O'Sullivan D, Geltink RIK, Curtis JD, Chang CH, Sanin DE, Qiu J, Kretz O, Braas D, van der Windt GJW, et al.: **Mitochondrial Dynamics Controls T Cell Fate through Metabolic Programming**. *Cell* 2016, **166**:63-76.
19. Chen HC, Chan DC: **Mitochondrial dynamics-fusion, fission, movement, and mitophagy-in neurodegenerative diseases**. *Human Molecular Genetics* 2009, **18**:R169-R176.
20. Burman JL, Pickles S, Wang C, Sekine S, Vargas JNS, Zhang Z, Youle AM, Nezich CL, Wu X, Hammer JA, et al.: **Mitochondrial fission facilitates the selective mitophagy of protein aggregates**. *J Cell Biol* 2017, **216**:3231-3247.
21. Milner DJ, Mavroidis M, Weisleder N, Capetanaki Y: **Desmin cytoskeleton linked to muscle mitochondrial distribution and respiratory function**. *J Cell Biol* 2000, **150**:1283-1298.
22. Lee CH, Kim MS, Chung BM, Leahy DJ, Coulombe PA: **Structural basis for heteromeric assembly and perinuclear organization of keratin filaments**. *Nat Struct Mol Biol* 2012, **19**:707-715.
23. Feng X, Coulombe PA: **Complementary roles of specific cysteines in keratin 14 toward the assembly, organization, and dynamics of intermediate filaments in skin keratinocytes**. *J Biol Chem* 2015, **290**:22507-22519.
24. Lessard JC, Coulombe PA: **Keratin 16-null mice develop palmoplantar keratoderma, a hallmark feature of pachyonychia congenita and related disorders**. *J Invest Dermatol* 2012, **132**:1384-1391.
25. Leveille CF, Mikhaeil JS, Turner KD, Silvera S, Wilkinson J, Fajardo VA: **Mitochondrial cristae density: a dynamic entity that is critical for energy production and metabolic power in skeletal muscle**. *Journal of Physiology-London* 2017, **595**:2779-2780.
26. Cogliati S, Enriquez JA, Scorrano L: **Mitochondrial Cristae: Where Beauty Meets Functionality**. *Trends Biochem Sci* 2016, **41**:261-273.
27. Buck MD, O'Sullivan D, Pearce EL: **T cell metabolism drives immunity**. *Journal of Experimental Medicine* 2015, **212**:1345-1360.
28. Ford ML, Bromberg JM: **Fueling Memory: How Cellular Metabolism Drives T Cell Immunity**. *American Journal of Transplantation* 2014, **14**:1953-1953.
29. Guo CY, Sun L, Chen XP, Zhang DS: **Oxidative stress, mitochondrial damage and neurodegenerative diseases**. *Neural Regeneration Research* 2013, **8**:2003-2014.
30. Zorov DB, Juhaszova M, Sollott SJ: **Mitochondrial Reactive Oxygen Species (Ros) and Ros-Induced Ros Release**. *Physiological Reviews* 2014, **94**:909-950.
31. Kalogeris T, Bao YM, Korthuis RJ: **Mitochondrial reactive oxygen species: A double edged sword in ischemia/reperfusion vs preconditioning**. *Redox Biology* 2014, **2**:702-714.
32. Bornhovd C, Vogel F, Neupert W, Reichert AS: **Mitochondrial membrane potential is dependent on the oligomeric state of F1F0-ATP synthase supracomplexes**. *Journal of Biological Chemistry* 2006, **281**:13990-13998.
33. Chernoivanenko IS, Matveeva EA, Gelfand VI, Goldman RD, Minin AA: **Mitochondrial membrane potential is regulated by vimentin intermediate filaments**. *FASEB J* 2015, **29**:820-827.

34. Chen H, Chan D: **Control of Mitochondrial Function by Fusion and Fission**. *Biophysical Journal* 2017, **112**:179a-179a.
35. Anso E, Mullen AR, Felsher DW, Mates JM, Deberardinis RJ, Chandel NS: **Metabolic changes in cancer cells upon suppression of MYC**. *Cancer Metab* 2013, **1**:7.
36. Hamanaka RB, Chandel NS: **Mitochondrial metabolism as a regulator of keratinocyte differentiation**. *Cell Logist* 2013, **3**:e25456.
37. Ott M, Gogvadze V, Orrenius S, Zhivotovsky B: **Mitochondria, oxidative stress and cell death**. *Apoptosis* 2007, **12**:913-922.
38. Samudio I, Konopleva M, Hail N, Shi YX, McQueen T, Hsu T, Evans R, Honda T, Gribble GW, Sporn M, et al.: **2-cyano-3,12-dioxooleana-1,9-dien-28-imidazolide (CDDO-Im) directly targets mitochondrial glutathione to induce apoptosis in pancreatic cancer**. *Journal of Biological Chemistry* 2005, **280**:36273-36282.
39. Wong P, Coulombe PA: **Loss of keratin 6 (K6) proteins reveals a function for intermediate filaments during wound repair**. *J Cell Biol* 2003, **163**:327-337.
40. Wang F, Chen S, Liu HB, Parent CA, Coulombe PA: **Keratin 6 regulates collective keratinocyte migration by altering cell-cell and cell-matrix adhesion**. *J Cell Biol* 2018, **217**:4314-4330.
41. Zieman AG, Poll BG, Ma J, Coulombe PA: **Altered keratinocyte differentiation is an early driver of keratin mutation-based palmoplantar keratoderma**. *Hum Mol Genet* 2019, **28**:2255-2270.
42. Kerns ML, Hakim JMC, Zieman A, Lu RG, Coulombe PA: **Sexual Dimorphism in Response to an NRF2 Inducer in a Model for Pachyonychia Congenita**. *Journal of Investigative Dermatology* 2018, **138**:1094-1100.
43. Zieman AG, Coulombe PA: **Pathophysiology of pachyonychia congenita-associated palmoplantar keratoderma: New insight into skin epithelial homeostasis and avenues for treatment**. *Br J Dermatol* 2019.
44. Hamanaka RB, Glasauer A, Hoover P, Yang S, Blatt H, Mullen AR, Getsios S, Gottardi CJ, DeBerardinis RJ, Lavker RM, et al.: **Mitochondrial reactive oxygen species promote epidermal differentiation and hair follicle development**. *Sci Signal* 2013, **6**:ra8.
45. Rath E, Moschetta A, Haller D: **Mitochondrial function - gatekeeper of intestinal epithelial cell homeostasis**. *Nat Rev Gastroenterol Hepatol* 2018, **15**:497-516.
46. Mironov SL, Symonchuk N: **ER vesicles and mitochondria move and communicate at synapses**. *J Cell Sci* 2006, **119**:4926-4934.
47. Yu C, Wang Y, Peng J, Shen Q, Chen M, Tang W, Li X, Cai C, Wang B, Cai S, et al.: **Mitochondrial calcium uniporter as a target of microRNA-340 and promoter of metastasis via enhancing the Warburg effect**. *Oncotarget* 2017, **8**:83831-83844.
48. da Silva AF, Mariotti FR, Maximo V, Campello S: **Mitochondria dynamism: of shape, transport and cell migration**. *Cell Mol Life Sci* 2014, **71**:2313-2324.
49. Boldogh IR, Pon LA: **Mitochondria on the move**. *Trends Cell Biol* 2007, **17**:502-510.
50. Desai SP, Bhatia SN, Toner M, Irimia D: **Mitochondrial localization and the persistent migration of epithelial cancer cells**. *Biophys J* 2013, **104**:2077-2088.
51. Altieri DC: **Mitochondria on the move: emerging paradigms of organelle trafficking in tumour plasticity and metastasis**. *Br J Cancer* 2017, **117**:301-305.
52. Matveeva EA, Venkova LS, Chernoivanenko IS, Minin AA: **Vimentin is involved in regulation of mitochondrial motility and membrane potential by Rac1**. *Biol Open* 2015, **4**:1290-1297.

53. Schwarz N, Leube RE: **Intermediate Filaments as Organizers of Cellular Space: How They Affect Mitochondrial Structure and Function**. *Cells* 2016, **5**.
54. StraubeWest K, Loomis PA, Opal P, Goldman RD: **Alterations in neural intermediate filament organization: Functional implications and the induction of pathological changes related to motor neuron disease**. *Journal of Cell Science* 1996, **109**:2319-2329.
55. David G, Barrett JN, Barrett EF: **Evidence that mitochondria buffer physiological Ca2+ loads in lizard motor nerve terminals**. *Journal of Physiology-London* 1998, **509**:59-65.
56. Wagner OI, Lifshitz J, Janmey PA, Linden M, McIntosh TK, Leterrier JF: **Mechanisms of mitochondria-neurofilament interactions**. *Journal of Neuroscience* 2003, **23**:9046-9058.
57. Wang F, Zieman A, Coulombe PA: **Skin Keratins**. *Methods Enzymol* 2016, **568**:303-350.

Figure Legends

Figure 1. (A-B) Representative transmission electron microscopy micrographs depicting the ultrastructure of mitochondria in E18.5 back skin from *WT* and *Krt6a/Krt6b* null littermates. Six pups were analyzed from each genotype. Arrows point to regions that are representative of the disorganized cristae observed in *Krt6a/Krt6b* null mitochondria. Bars equal 200nm. (C-D) Analysis of specific mRNA transcripts in total RNA samples. Keratinocytes were isolated from P1 *WT* and *Krt6a/Krt6b* null littermates and seeded at equal cell density for culture. Total RNA was isolated and analyzed. Gene expression of mitochondrial markers were normalized to corresponding 18S expression in each sample. n=6 and 3 independent experiments were performed. Student's t test was used with significance set at $p<0.05$.

Figure 2. (A) Indirect immunofluorescence staining for K16 and pyruvate dehydrogenase (PDH) in keratinocytes isolated from P1 *WT Krt16* mouse strain and cultured in primary conditions. The images were acquired using an LSM 800 Airyscan mode. Bars equal 20μm. (B) Staining of PDH in newborn P1 *WT* and *Krt6a/Krt6b null* skin keratinocytes in primary culture. Dashed lines depict the cell periphery and nucleus. Graphs depict PDH signal intensity distribution in the cytoplasm, as the intensity fraction of the total intensity with respect to the distance from nucleus or the distance to the nucleus normalized to the spacing between nucleus and the cell boundary. The curves are the average intensity over 18 *Krt6a/Krt6b null* Cells and 34 *WT* cells Bars equal 20μm.

Figure 3. (A) A Seahorse analysis was performed using the FX96 analyzer using the Agilent protocol for mitochondrial stress assay (see Methods). 4×10^4 skin keratinocytes from P1 *WT*, *Krt6a/Krt6b* null and *Krt16* null mice were seeded in primary culture. Samples were normalized and mitochondrial basal respiration, maximal respiration and proton leak were determined *Krt6a/Krt6b* null and *Krt16* null each exhibited lower levels of these three parameters with no change in ATP production or spare respiratory capacity. n= 10-16 from 3 independent experiments. Student's t test was used with significance set at $p<0.05$. (B) Skin keratinocytes were isolated from P1 *WT* and *Krt6a/Krt6b* null littermates (left) or *WT* and *Krt16* null littermates (right) and cultured in primary conditions. 7×10^4 cells were seeded in a 96-well plate and labeled with 500nM of TMRE for 30 minutes, and fluorescence was then measured. Cells were normalized by measuring total DNA using CyQuant dye. n=5-20 from 3 independent experiments performed. Student's t test was used with significance set at $p<0.05$.

Figure 4. Live imaging studies. 50,000 skin keratinocytes were obtained from P1 *WT*, *Krt6a/Krt6b null* and *Krt16 null* mice and seeded for primary culture overnight. Cells were then labeled with 50nM of MitoTracker Red and live cell imaging was performed for 5 minutes to track labeled mitochondria of individual cells. The average speed of the tracked mitochondrial shapes with area between 1 um^2 and 10 um^2 was measured for each cell. There are 3 independent experiments and in each of them $n > 5$ cells. In the box plot, the scatter points represent each cell. The whiskers represent the range of the data and the box indicate the 25% to 75% percentile. The notch with the middle line indicates the median and the cross represents the outlier. In both box plots, p-value < 0.0001.

Figure 1. Steen et al.

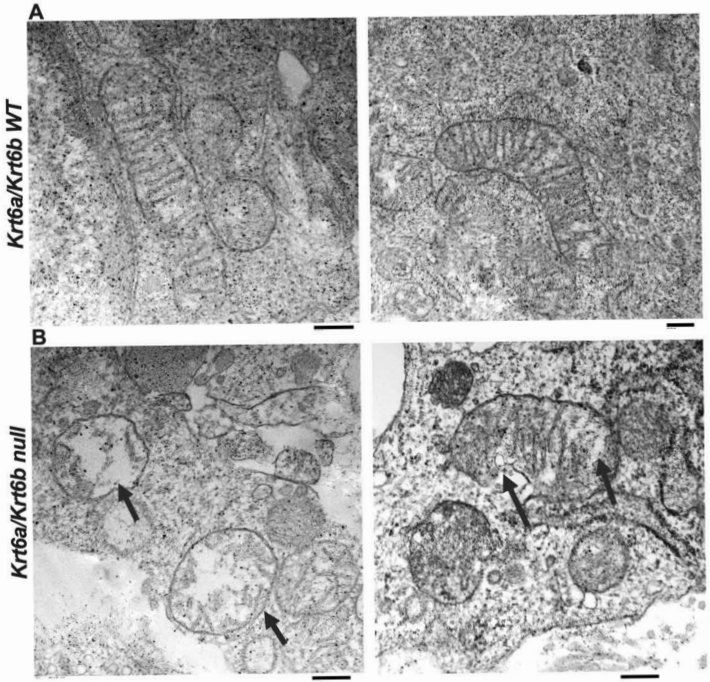

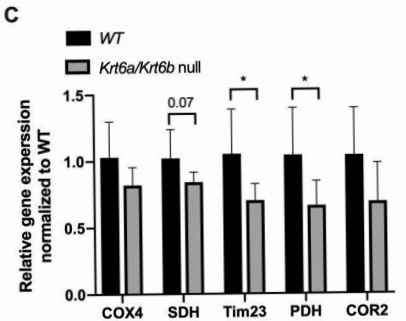

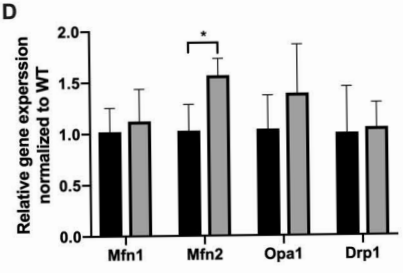

Figure 2. Steen et al.

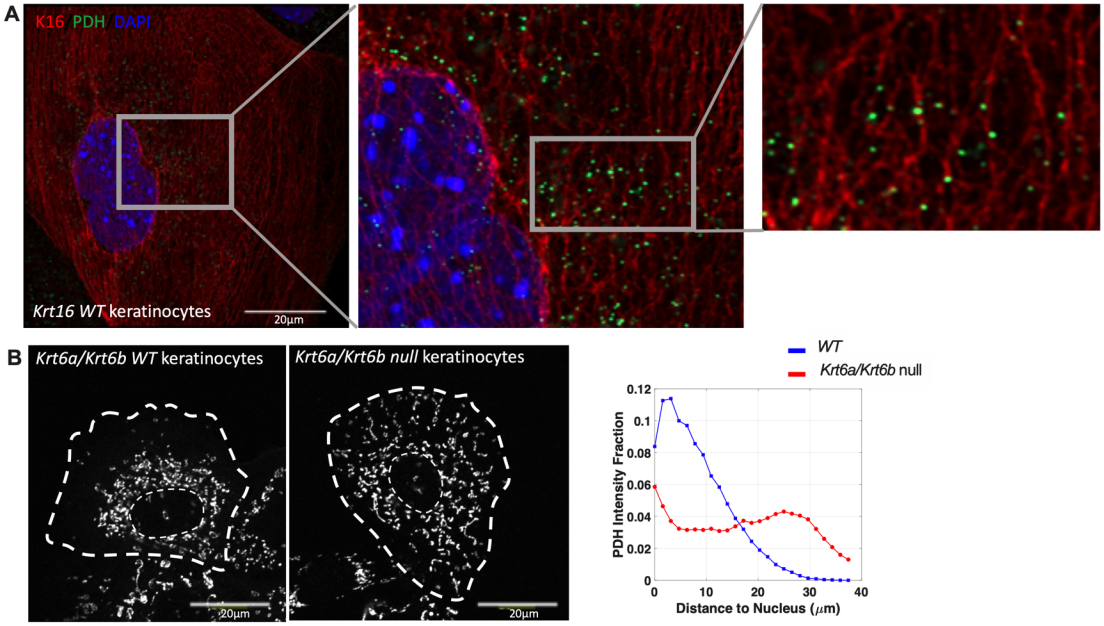

Figure 3. Steen et al.

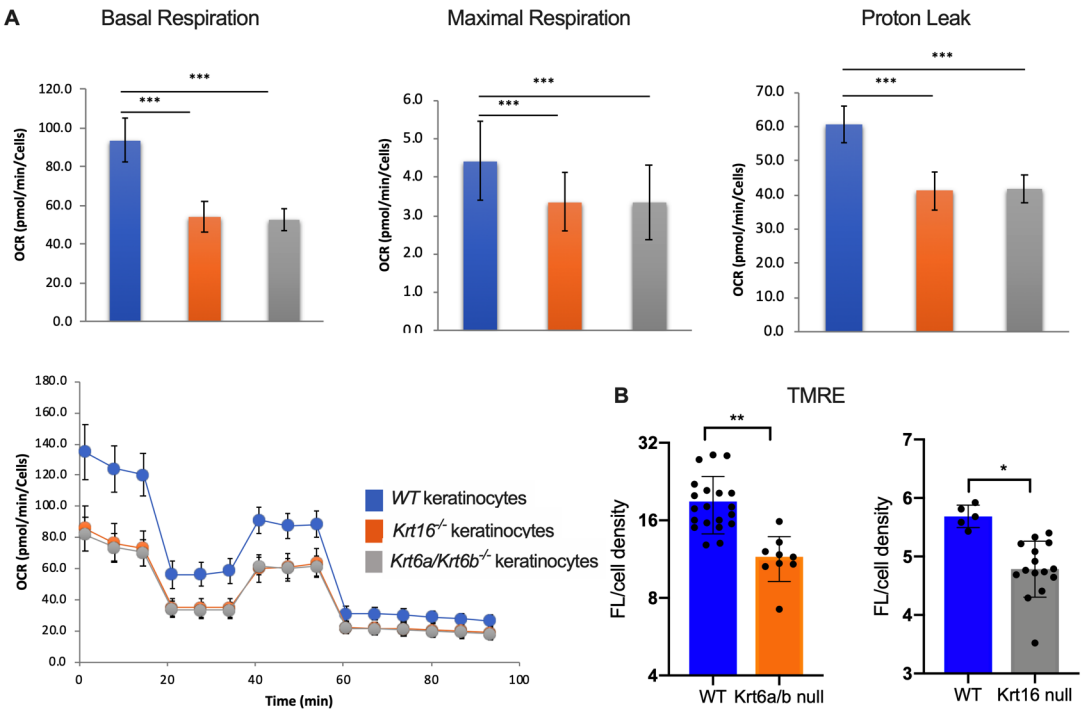

Figure 4. Steen et al.